PAPER • OPEN ACCESS

Protocols and methodologies for acquiring and analyzing critical-current versus longitudinal-strain data in $Bi_2Sr_2CaCu_2O_{8+x}$ wires

To cite this article: Najib Cheggour and Emsley L Marks 2025 *Supercond. Sci. Technol.* **38** 015012

OPEN ACCESS
IOP Publishing

Superconductor Science and Technology

Supercond. Sci. Technol. **38** (2025) 015012 (15pp)

https://doi.org/10.1088/1361-6668/ad9ad9

Protocols and methodologies for acquiring and analyzing critical-current versus longitudinal-strain data in $Bi_2Sr_2CaCu_2O_{8+x}$ wires

Najib Cheggour[1,*] **and Emsley L Marks**[2]

[1] Applied Superconductivity Center, National High Magnetic Field Laboratory, Florida State University, Tallahassee, FL 32310, United States of America
[2] Magnet Science & Technology, National High Magnetic Field Laboratory, Florida State University, Tallahassee, FL 32310, United States of America

E-mail: ncheggour@asc.magnet.fsu.edu

Received 7 August 2024, revised 22 November 2024
Accepted for publication 5 December 2024
Published 13 December 2024

Abstract

In the literature on $Bi_2Sr_2CaCu_2O_{8+x}$ (Bi-2212) superconducting wires, it is evident that measurement protocols for transport critical-current I_c versus longitudinal strain ε and definitions of the so-called 'strain limit' are generally dissimilar. Yet, values obtained for the 'strain limit' are frequently assimilated to being those of the irreversible strain limit ε_{irr}, regardless of the I_c degradation-criterion used to define it. In effect, ε_{irr} should correspond specifically to the $I_c(\varepsilon)$ irreversibility *onset*, where crack formation in Bi-2212 filaments presumably starts. Because $I_c(\varepsilon)$ degradation remains progressive over a fairly wide strain range beyond ε_{irr}, the different I_c degradation-criteria in use do not yield to the same result and, thus, are not equivalent from metrology perspective. Indeed, in studying densified samples of a modern Bi-2212 round wire, we found $\varepsilon_{irr} \approx 0.4\%$ and $\varepsilon_{5\%} \approx 0.6\%$ ($\varepsilon_{5\%}$ being the strain where I_c degrades by 5%). In this paper, we outline and suggest $I_c(\varepsilon)$-measurement protocols and data-analysis methodologies in the hope to converge the various approaches taken for studying Bi-2212 strain properties and, thus, remove related result discrepancies. A unified approach would enable more objective data comparisons among laboratories and among different Bi-2212 conductors. It would pave the way for more rigorous studies of effects potentially associated with wire design, powder, heat treatments, and other such parameters on the conductor's strain properties.

Keywords: Bi-2212, critical current, data analysis, irreversible strain effects, methodologies, protocols, strain limits

* Author to whom any correspondence should be addressed.

1. Introduction

The potential of the superconducting $Bi_2Sr_2CaCu_2O_{8+x}$ multifilamentary round wires (Bi-2212) for various magnet applications is very promising [1, 2]. With it being brittle, as most superconductors are, electromechanical investigations to understand stress and strain effects remain essential for the conductor development and its applications. Such studies include transport critical-current I_c dependence on longitudinal strain ε.

When data resolution is not sufficiently high to identify the onset of $I_c(\varepsilon)$ irreversibility, presumably corresponding to the initiation of crack formation in Bi-2212 filaments that lead to permanent degradation of I_c, I_c-degradation criteria are often used to define the conductor's strain limit—a characteristic strain typically considered for designing magnets. These criteria may be convenient but their usage in data analysis does not appear to be uniform among laboratories generating such data. Even the labeling of the strain limit is not uniform. There is a need to reevaluate how strain data are acquired and analyzed for Bi-2212 conductors, how the strain limit is defined and, to the extent possible, adopt a unified approach in order to achieve a better consistency in the data reported.

In this paper, we investigate I_c dependence on tensile and compressive longitudinal strain ε in densified samples of a modern Bi-2212 wire. We apply different modes of measurements with varying severity to evaluate the influence of these modes on the data obtained. We introduce protocols and methodologies for generating and analyzing Bi-2212 strain data in the hope to converge approaches taken in other labs. If considered, these protocols and methodologies, or similar, may make data comparisons more informative. By eliminating potential sources of data inconsistencies, they may also provide a solid platform for more rigorous studies of the causality between strain effects and the conductor design, fabrication, and heat-treatment.

2. Viewpoint on Bi-2212 strain properties reported in literature

Strain measurements allow examining whether I_c has a reversible dependence on ε, the form and magnitude of this dependence, and at what characteristic strains irreversible I_c degradation initiates and grows to potentially unsafe levels.

Earlier studies showed that, at moderate longitudinal tensile strain, I_c decreases linearly vs. ε following a very small slope α. The decrease of I_c becomes pronounced when tensile strain is increased beyond a certain limit taken as characterizing the resilience of the conductor to strain. In longitudinal compressive strain, I_c degrades almost immediately but at a rate that is less severe than in tension beyond the strain limit. This generic behavior was summarized in two descriptive strain models [3, 4].

Early reports by Ten Haken *et al* thoroughly discussed reversibility of I_c with tensile strain in light of the very small values of the slope α (of the order of -4% per% strain) and limitations of measurement resolution and reproducibility that make it difficult to detect reversibility of strain effects within such a weak $I_c(\varepsilon)$ dependence [5]. In fact, they concluded that I_c reduction with strain is completely irreversible in Bi-2212 conductors [4, 5]. They set a criterion of 2% I_c degradation for defining a strain limit and labeled it $\varepsilon_{2\%}$ [4, 5], not ε_{irr}—the irreversible strain limit. Indeed, ε_{irr} labeling should be reserved for a characteristic strain delimiting a domain where $I_c(\varepsilon)$ dependence in a superconductor is reversible, originating solely from elastic deformations of the material's crystal lattice parameters with strain, not convoluted with extrinsic effects originating from cracking of the brittle superconductor (this should be the case for any superconductor material for that matter, not just Bi-2212). They used $\varepsilon_{2\%}$ instead because there was no experimental evidence for reversibility of strain effects on I_c, even though by x-ray diffraction they showed an elastic deformation of Bi-2212 grains within a strain range between -0.1% and $+0.2\%$ along the lattice c-axis at room temperature [6]. Irreversibility of $I_c(\varepsilon)$ was the backbone of their descriptive strain model [4]. Later, Cheggour *et al* reported a reversible effect of tensile strain on I_c up to $\varepsilon_{\text{irr}} \approx 0.3\%$ in non-densified Bi-2212 samples, though this reversibility was not observed in all samples investigated in that work [3]. In axial compression, strain effect was reported to be irreversible [3–5] and buckling of Bi-2212 grains was identified as a failure mode in compression [3].

Some literature either relaxed the degradation criterion to 5% or did not set an explicit criterion. Some reports labeled the strain limit as ε_{irr}, without showing evidence for $I_c(\varepsilon)$ reversibility, or combined the labeling of the irreversible strain limit and degradation-percent strain limit into a hybrid label, such as $\varepsilon_{\text{irr-5\%}}$ for example. Such labeling can give the false impression that $I_c(\varepsilon)$ remains reversible up until 5% I_c reduction.

Also, it is not always clear what reference point the degradation is calculated against, whether it corresponds to the total I_c degradation at a loaded strain point with respect to the virgin value I_{c0} at zero applied strain, or to the relative I_c degradation at an unstrained or a partially strained state with respect to I_{c0} (i.e. after the sample has been loaded and then fully or partially unloaded, respectively).

On first sight, these concerns might look insignificant. Yet, differences in the values reported for the 'strain limit' in literature do exist. They vary between 0.3% and 0. 6% or even higher [3–5, 7–11]. The lack of a unified definition for this limit and how it is extracted from the data, and the lack of well-defined measurement protocols may be significant contributors to these differences. It would be useful to identify what part of these variations in the results is related to the specific conductors measured in different labs, and what part stems from differences in the definition used for the strain limit, data-analysis methods, or protocols and measurement techniques.

Differences in sensitivity among strain apparatuses may be a challenge against adopting a unique definition for the strain limit and, in fact, we may still need to identify which strain-limit definition is most relevant to applications. Nonetheless, establishing measurement protocols and explicitly declaring the criterion used in data analysis will bring clarity and consistency in strain data generated on Bi-2212 conductors. In this paper, we intent to shed some light on this metrology topic. For more objectivity, we will mostly use the term 'characteristic strain' instead of 'strain limit'.

3. Experimental

3.1. Conductor investigated and over-pressure heat-treatment (OP-HT) used

Measurements were made on a Bi-2212 multifilamentary round wire made of 18 bundles of 85 Bi-2212 filaments each and restacked in a reinforced Ag-0.2 wt.% Mg outer sheath. The conductor was manufactured by Bruker-OST by use of the powder-in-tube technique. The conductor (billet number PMM180410) had a final diameter of 1.0 mm and was untwisted. The Bi-2212 precursor powder was fabricated by Engi–Mat by use of the nanospray combustion chemical vapor condensation method.

Each of the samples investigated was wound on an Inconel-600 mandrel for OP-HT [12–17]. The mandrel had a diameter of 25 mm, a length close to 150 mm, and had three grooves to hold up to three samples at once. Sample length was 2.2 m approximately, and its ends were sealed to enable full densification and to prevent leakage of material during heat treatment.

Profiles of OP-HT had multiple stages at various dwelling temperatures, times, and ramp rates, such as in [1] for example. We used 50-bar overpressure to obtain highly densified samples. The heat treatment was performed at a maximum temperature of 889 °C. Time in the melt was 2.2 h approximately. Reacted samples had no leakages. In the appendices, to make specific points regarding data analysis and measurement modes, we will also present examples of data obtained on a non-densified sample that received an OP-HT at 5 bar.

3.2. Strain device

The device for applying longitudinal strain to the sample is a Walters spring made of cold-worked and precipitate hardened Cu-2%Be alloy [18–20]. The spring has the same diameter and pitch (6.4 mm) as the reaction mandrels. It has four turns in the middle section and is permanently attached to a Cu lug at each end (this whole assembly is referred to as the spring). This strain device has a wide elastic–strain range from -1% to $+1\%$ as demonstrated through strain-gauge calibrations.

Suitability of Cu–Be material for making strain devices to test Bi-2212 conductors goes beyond just its large elastic strain range and its high solderability [3, 19]. Indeed, Sugano *et al* reported that the thermal contraction of this material matches that of a typical Bi-2212 composite wire (like the one studied herein) extremely well [11]. When cooled from room temperature to 5 K, the mismatch in thermal contraction is insignificant (within 0.01%) [11]. Hence, a Bi-2212 conductor sample soldered onto a Cu–Be holder should experience practically no pre-strain upon cooling to liquid He temperature. This is greatly advantageous, particularly because $I_c(\varepsilon)$ of Bi-2212 does not have a peak that can be used as a strain reference like in Nb_3Sn conductors for example [21, 22]. It has been highlighted subsequently by other authors who contrasted Cu–Be with Ti–Al–V alloy also used for making strain devices such as a Walters spring, a U-bending spring, or a Pacman [7, 9, 10]. This thermal-contraction matching is a rare coincidence that should make Cu–Be the first-choice material for fabricating strain devices for measuring Bi-2212 wires.

A jig is used to firmly connect our spring to the mandrel (containing reacted samples) such that the two are well aligned with each other longitudinally [19]. By gently turning one end of the sample that is free to move along the groove housing it, the sample is progressively transferred from the reaction mandrel onto the spring. Several turns at both sample ends are cut and repositioned next to the new sample ends for splicing them together. Doubling the sample end turns is useful to minimize current-contact resistance. It prevents potential temperature rise and inhibits voltages along the measured sections during transfer of current into the sample ends. The sample is gently positioned on the spring and pieces of a thin steel wire are wound at two locations at each end of the spring to keep the sample and its splices attached together and to the spring. The mandrel and spring are then disconnected. Heater cartridges and thermocouples are inserted into the spring (from its ends) to solder the sample onto the spring at ≈200 °C by use of Pb37%–Sn63% eutectic solder. Multiple pairs of voltage taps are attached to the sample at various locations. The principal ones are three pairs (taps 1, 2, and 3) attached to the sample section laid on the spring turns, each pair monitoring one sample turn (or segment) ≈ 8 cm in length. Use of temperature-controlled heater cartridges allows for more uniform heating and cooling of the sample/spring assembly such that the sample experiences minimal thermal-strain during soldering. After this operation, the spring is then attached to the strain apparatus and current contacts and instrumentation connections are made.

The apparatus is inserted into a superconducting solenoid magnet. Measurements of the sample current vs. voltage (I–V) are made in a lightly pressurized liquid He at 4.26 K—slightly above the lab's He boiling point—for the purpose of controlling sample temperature during measurements. Vapor pressure of liquid He is controlled by use of a throttle valve inserted between the apparatus/cryostat and the He recovery line. This ensures that the sample temperature stays constant during every I–V curve measurement, independently of the amount of current injected in the sample, and throughout the day even when ambient atmospheric pressure happens to change. We follow this procedure systematically for measuring strain properties of various superconducting materials [21–24], though it is not really needed for Bi-2212 material, given its very high critical-temperature T_c, when measurements are done at a low reduced temperature $-T/T_c \approx 0.05$ in this work. The sample is subjected to a magnetic field of 16 T, perpendicular to the current and oriented such that the Lorentz force applied to the sample is directed inward. The sample is thus protected against the Lorentz force by the Walters spring.

By twisting one spring end with respect to the other end, the spring's outer surface to which the sample is attached is subjected to either a tensile or a compressive axial strain. The angular twist applied to the spring is measured by means of a protractor attached to the top end of the spring by a connecting tube. A needle to measure the angle on the protractor is attached to the bottom end of the spring by a connecting rod. Both protractor and needle emerge near the top end of the apparatus, outside of the magnet cryostat, and can be read easily by the operator. The relationship between angular displacement and strain at the surface of the spring was obtained through a calibration, prior to any sample mounting, where several strain gauges were attached to the outer surface of the spring (strain gauges were removed after calibration). This calibration revealed a linear, reproducible, and reversible dependence of strain on the angular twist, and homogeneous strain along the spring turns [19]. Thus, during $I_c(\varepsilon)$ measurements, we use the angular displacement to determine the sample strain.

When a round-wire sample is mounted on the spring, and for a given angular twist applied between the spring ends, there is a strain gradient from the sample line in contact with the outer surface of the spring to the outermost sample line, i.e. along the transverse cross-section of the round-wire sample. This gradient depends on the diameters and Young's moduli of the Cu–Be spring and sample. Because of this gradient, we quote strain at the sample's central axis/plane around which the majority of the Bi-2212 filaments are clustered, not at the outer surface of the spring. In comparison to the quoted strain, for the studied conductor, the outermost Bi-2212 filaments and the ones closest to the outer surface of the spring experience strains about 7% higher and 7% lower, respectively, given the relatively large wire diameter (1 mm). However, this gradient is significantly less (±4.5% max) for the majority of the Bi-2212 filaments. This gradient is part of experimental uncertainties in estimating applied strain.

Values of I_c reported herein were determined from *I–V* curves at the electric field criterion E_c of 0.1 μV cm^{-1}. To evaluate effects of E_c on determining characteristic strains, I_c values were also analyzed for 1 μV cm^{-1} where indicated. The *n-value* index was calculated for the portion of the *I–V* curve between 0.07 and 0.2 μV cm^{-1}. Expanded uncertainties due to random effects in estimating I_c, ε_{irr} (and other characteristic strains), and *n-value* were 2%, 0.04% strain, and 3%, respectively.

Our apparatus is of the category of strain devices where the sample, in coiled or straight shape, is soldered to a beam that is either a Walters spring, Pacman, or U-shaped. Despite soldering Bi-2212 sample to the beam, the sample should in principle be in a near strain-free state upon cooling to liquid He temperature if the beam is made of Cu-2%Be alloy, as explained above, and precautions not to strain the sample are taken during sample mounting. This sort of apparatuses allows for measuring strain but not stress applied to the sample, nevertheless. The other category of strain apparatuses accommodates free-standing straight samples, which should be in a strain-free state upon cooling to liquid He temperature if there is no friction that would prevent the sample from contracting freely. It offers the possibility of measuring both strain and stress applied to the sample. Each type of apparatuses has advantages and disadvantages relating to measurement sensitivity, current-transfer voltages, protection against the Lorentz force, mechanical stability, and other experimental aspects. Descriptions of these techniques can be found in literature [6, 8, 10, 18, 19, 25, 26]. We emphasize that this work is not intended to compare various strain-measurement apparatuses or promote one over another. The overarching goal is to highlight the importance of unifying $I_c(\varepsilon)$-measurement protocols and data-analysis methodologies for Bi-2212 conductors in particular, *irrespective* of the type of strain apparatus used.

3.3. Modes of strain measurements

We used three modes of measurements that we describe as follow:

- Monotonic-loading mode (I): strain was monotonically increased each time by a constant and small amount close to 0.02% and an *I–V* curve was measured for each strain value. Measurements were carried out until the sample was almost completely damaged (I_c close to 0 A). For measurements in compression, the same protocol was followed except that the strain increment was about −0.02%.
- Load/partial-unload mode (II): first, strain was monotonically increased by the same amount of 0.02%. Starting from $\varepsilon \approx 0.18\%$, strain was partially unloaded by a constant step $\Delta\varepsilon$ but not brought back to 0%. Measurements were conducted in both the loaded and partially-unloaded sample states to check reversibility of I_c vs. ε. Thereafter, strain was increased to a slightly higher value and measurements taken, then strain was partially unloaded again by the same $\Delta\varepsilon$ and measurements taken. This was repeated multiple times while incrementally increasing ε until the sample was mostly damaged. This mode subjects the sample to some fatigue cycles though not in the classical way of fatigue testing. The strain step $\Delta\varepsilon$ was kept constant throughout the measurements of a given sample and was either −0.11% or −0.15% for different samples. Measurements in [3] were also conducted in mode II.
- Load/full-unload mode (III): this was similar to the load/partial-unload mode except that applied strain was brought back to 0% after every strain loading. In this case, the unloading step $\Delta\varepsilon$ increased each time as ε was increased. This mode also subjects the sample to some fatigue cycles and may be the most severe among the three modes.

These strain testing modes may not simulate exactly the conditions in magnet applications, which conditions may vary broadly. The intent is to test samples in well-defined modes and determine if and how these modes influence the results.

Nomenclature used for the samples measured in tension is 'mode'-'sample number'. For example, sample I-1 was sample 1 measured in mode I (in tension). Samples measured in compression (all in mode I) are labeled I-c 'sample number' (for example, sample I-c1).

4. Methodologies for data analysis and results

We propose methodologies for analyzing data depending on the measurement mode used. Detailed datasets are recommended to improve accuracy of the analysis. We measured five samples in total, three sample turns (or segments) for each. In the following, we present detailed and representative examples of the experimental results, along with data-analysis methodologies and outcome (also see [27]).

4.1. Tensile strain effects

4.1.1. Modes I and II. All data presented in this and the following section 4.1.2 use I_c values obtained at 0.1 μV cm^{-1}. Data obtained at 1 μV cm^{-1} will be shown in section 4.1.4 to evaluate the effect of E_c on the results.

In mode I (explained above), strain is not released during measurements and so it does not allow to check I_c reversibility with ε. First, we show the case of mode II. Conclusions from this mode will help us analyze data of Mode I.

An example of the results obtained in mode II is shown in figure 1 for sample II-2. The solid and empty circle symbols plotted on the left Y-axis represent $I_c(\varepsilon)$ when the sample was loaded and partially unloaded and are indicated by a pair of unprimed and primed letters, respectively. For example, A′ is the partially unloaded point that corresponds to the loaded point A. The unloading strain step $\Delta\varepsilon$ was -0.15% throughout measurements of sample II-2, and -0.11% for sample II-1 also measured in this mode (table 1).

We used two methods to analyze the data obtained in mode II. The first method consists of calculating the relative degradation $(\Delta I_c/I_c)_R$ that represents I_c drop at a given (partially) unloaded strain point relative to I_c at the loaded strain point that has the same applied strain (for example points S′ and K in figure 1(a)), and assigning to it the strain value of the corresponding loaded point (S in the previous example). This is similar to the method used for Nb_3Sn conductors [28], adapted here for Bi-2212 conductors. $(\Delta I_c/I_c)_R$ dependence on strain is plotted on the right Y-axis by use of rectangular symbols (figure 1(a)). It exhibited three distinct domains: First, $(\Delta I_c/I_c)_R$ was flat and very close to zero, indicating reversibility or near reversibility of I_c as a function ε. The value of $(\Delta I_c/I_c)_R$ at this plateau, which measures the average shift of the unloaded curve from the loaded curve in the moderate strain range, is -0.17% for the example presented in figure 1(a). This shift varied from -0.06% to -0.17% amongst the six taps of samples II-1 and II-2, averaging for the three taps of each sample -0.10% and -0.12%, respectively. The example in figure 1(a) represents the high end of this shift, yet it is very small. Hence, the behavior of $I_c(\varepsilon)$ is essentially reversible in this strain region. After the plateau, $(\Delta I_c/I_c)_R$ started decreasing gradually over a relatively narrow strain range before dropping at a significantly steeper rate when strain is increased further. These same three domains have been observed invariably for the two samples measured in this mode, for all their six taps.

This detailed analysis revealed not just one but two characteristic strain values, ε_{irr} and ε_{rate} (marked by arrows in figure 1(a)), delimiting the intersections of the three domains. ε_{irr} is the strain at the end of $I_c(\varepsilon)$ reversibility and the onset of I_c irreversible decrease, and ε_{rate} is strain marking the first noticeable change in I_c degradation rate.

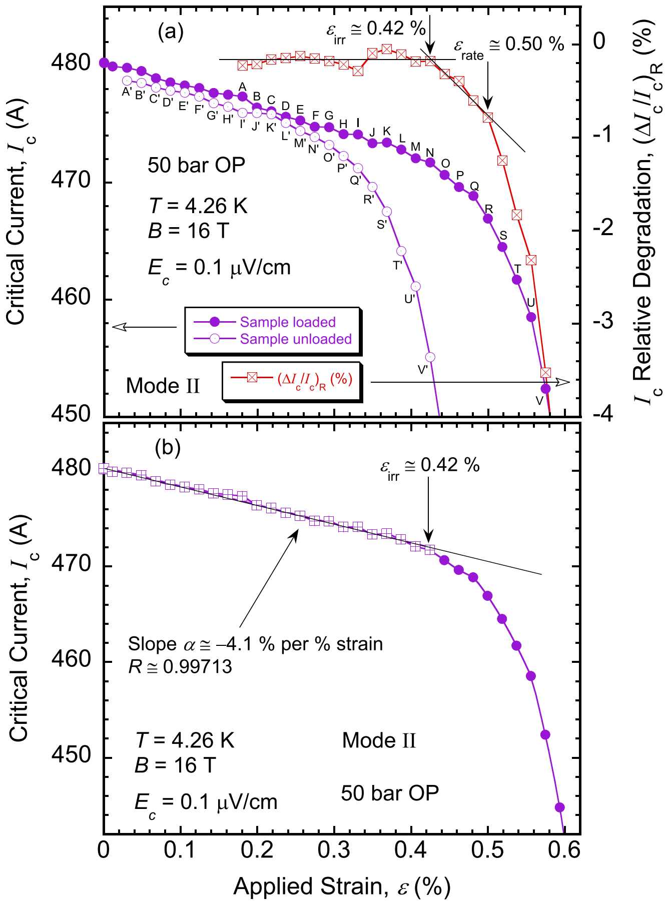

Figure 1. Example of $I_c(\varepsilon)$ results and related data analysis obtained on densified Bi-2212 sample II-2 in the load/partial-unload mode (II) at 16 T, 4.26 K, and 0.1 μV cm^{-1}. (a) $I_c(\varepsilon)$ data for the sample when loaded and partially-unloaded are plotted on the left Y-axis. Each pair of unprimed and primed letters indicates a loaded strain point (solid symbol) and its corresponding partially unloaded strain point (empty circle symbol), respectively (for example points A and A′). Degradation $(\Delta I_c/I_c)_R$ for an unloaded point relative to the loaded point corresponding to the same applied strain (for example points S′ and K), is plotted on the right Y-axis as a function of ε by use of square symbols. This method of data analysis revealed three distinct regions bordered by two characteristic strains ε_{irr} and ε_{rate} that correspond to the onset of irreversibility and the first noticeable change of I_c-degradation rate, respectively. (b) Linear fit of the loaded points to determine the onset of deviation from linearity, defined as ε_{irr}. Points maximizing the correlation factor R of the linear fit are plotted by use of square symbols for clarity. Method of the data analysis in (a) that uses both loaded and unloaded points and that in (b) that uses loaded points only yield the same results for ε_{irr}. Value of the slope α of $I_c(\varepsilon)$ dependence within the reversible regime is indicated in the graph.

The relative degradation $(\Delta I_c/I_c)_R$ at ε_{rate} is less than -1% (figure 1(a)) for all six taps, whereas the total degradation $(\Delta I_c/I_{c0})_T$—with respect to the first value I_{c0} at zero strain—at ε_{rate} is between -2.5% to -3% for both samples II-1 and II-2 (table 1). The 2% degradation criterion puts $\varepsilon_{2\%}$ slightly higher than ε_{irr}, where the total degradation $(\Delta I_c/I_{c0})_T$ is around -1.7% on average in mode II (table 1), and lower than ε_{rate}. The 5% degradation criterion puts the characteristic strain $\varepsilon_{5\%}$ significantly higher than ε_{irr}.

Table 1. Characteristic strains and related parameters obtained on densified Bi-2212 samples measured in modes I, II, and III at $E_c = 0.1\ \mu$V cm^{-1}.

Monotonic-loading mode (I)									
50 bar OP-HT		Slope α (% per % strain)	Coefficient R	ε_{irr} (%)	$(\Delta I_c/I_{c0})_T$ at ε_{irr} (%)	$\varepsilon_{2\%}$ (%)	ε_{rate} (%)	$(\Delta I_c/I_{c0})_T$ at ε_{rate} (%)	$\varepsilon_{5\%}$ (%)
Sample I-1	Tap 1	–4.1	0.99846	0.39	–1.5	0.45	—	—	0.58
$\Delta\varepsilon = 0\%$	Tap 2	–3.9	0.99760	0.37	–1.5	0.42	—	—	0.55
	Tap 3[a]	–3.9	0.99877	0.46	–1.4	0.53	—	—	0.60
Load/Partial-unload mode (II)									
50 bar OP-HT		Slope α (% per % strain)	Coefficient R	ε_{irr} (%)	$(\Delta I_c/I_{c0})_T$ at ε_{irr} (%)	$\varepsilon_{2\%}$ (%)	ε_{rate} (%)	$(\Delta I_c/I_{c0})_T$ at ε_{rate} (%)	$\varepsilon_{5\%}$ (%)
Sample II-1	Tap 1	–4.0	0.99745	0.38	–1.6	0.44	0.53	–3.0	0.59
$\Delta\varepsilon = -0.11\%$	Tap 2	–4.1	0.99753	0.42	–1.8	0.45	0.51	–2.6	0.59
	Tap 3	–4.2	0.99859	0.41	–1.7	0.44	0.49	–2.5	0.57
Sample II-2	Tap 1	–4.1	0.99696	0.42	–1.8	0.44	0.50	–2.6	0.59
$\Delta\varepsilon = -0.15\%$	Tap 2	–4.1	0.99713	0.42	–1.8	0.44	0.50	–2.8	0.56
	Tap 3	–3.6	0.99458	0.46	–1.7	0.50	0.56	–2.6	0.62
Load/Full-unload mode (III)									
50 bar OP-HT		Slope α (% per % strain)	Coefficient R	ε_{onset} (%)	$(\Delta I_c/I_{c0})_T$ at ε_{onset} (%)	$\varepsilon_{2\%}$ (%)	ε_{rate} (%)	$(\Delta I_c/I_{c0})_T$ at ε_{rate} (%)	$\varepsilon_{5\%}$ (%)
Sample III-1	Tap 1	–5.5	0.99817	0.35	–1.9	0.36	0.45	–2.8	0.53
$\Delta\varepsilon$ variable	Tap 2	–5.5	0.99742	0.33	–1.8	0.36	0.42	–2.7	0.50
	Tap 3	–5.3	0.99853	0.41	–2.2	0.38	0.45	–2.7	0.51

[a] See appendix A.

The second method we used to analyze the data in figure 1 is applied to the loaded points only and examines the linearity of $I_c(\varepsilon)$ in the moderate strain range. A first selection of data points that can be fitted with a linear function was made and the correlation coefficient R of the least-square fit calculated. To refine the fit, some data points around the end of $I_c(\varepsilon)$ linear region were then either removed or added to the fit to maximize R. The results are shown in figure 1 (b). Data points selected that provide the best linear fit (i.e. maximum R) are plotted by use of square symbols to identify them better. The point where $I_c(\varepsilon)$ deviates from linearity is defined as ε_{irr}, considering that the onset of irreversibility plausibly triggers this deviation (we will discuss this point later). For improved accuracy of ε_{irr} determination, the density of data points acquired was made high. Values of ε_{irr} with this second method matched those obtained with the first method very well (figure 1), systematically for all the six taps, clearly validating this second analysis method that is much simpler and does not require any degradation criterion. This method does not need unloaded strain points either and so it potentially can be used to analyze data obtained in mode I.

Data of *n-value*(ε) are plotted in figure 2. We used the same nomenclature as in figure 1(a). The *n-value* is rather constant at first and its irreversibility onset seems located at the strain point N, which also corresponds to the end of *n-value*(ε) plateau. Thus, ε_{irr} is about 0.42%, consistent with the value obtained through the analysis of $I_c(\varepsilon)$ data, as in [3]. Nevertheless, the onset of irreversibility is not always clear from *n-value*(ε) and its determination is approximate as data are noisier than $I_c(\varepsilon)$. Moreover, in some cases we found that the drop of *n-value*(ε) lags that of $I_c(\varepsilon)$ to higher strain values. We will further discuss the *n-value* in the section addressing the compressive strain effects.

For mode I, the only way to analyze data is to use the linear fit method discussed above, assuming that $I_c(\varepsilon)$ behaves reversibly in this mode in the moderate strain range. An example for sample I-1 is given in figure 3 (also see table 1). Nonetheless, mode I does not provide the possibility to check $I_c(\varepsilon)$ reversibility nor to determine ε_{rate}. In fact, it is not always true that $I_c(\varepsilon)$ linearity is a proof for $I_c(\varepsilon)$ reversibility. An irreversible, yet linear, $I_c(\varepsilon)$ behavior is possible but is characterized by a steeper slope α than for when the behavior is reversible (see section 4.1.2 and [3]).

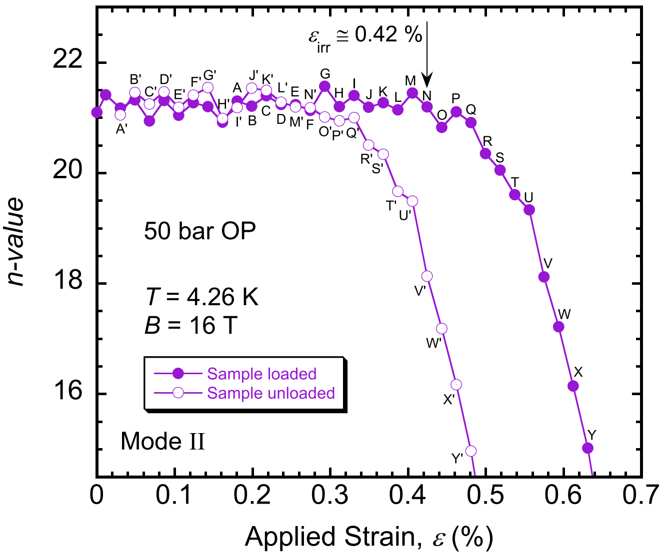

Figure 2. Example of *n-value*(ε) results obtained on densified Bi-2212 sample II-2 in the load/partial-unload mode (II) at 16 T and 4.26 K. Nomenclature used is the same as in figure 1(a) to relate data points of *n-value* and corresponding I_c. Irreversibility of *n-value*(ε) started at point N approximately, at the same ε_{irr} value as for $I_c(\varepsilon)$. Nevertheless, in other examples, *n-value*(ε) irreversible drop either lagged that of $I_c(\varepsilon)$ to higher strain values or was hard to define unambiguously.

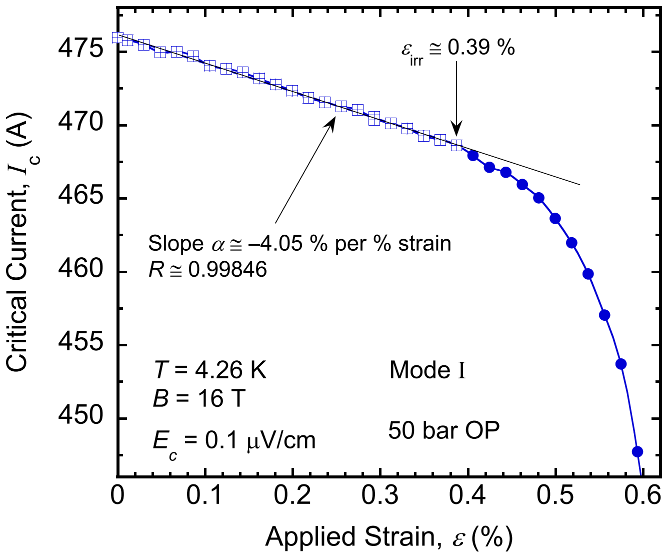

Figure 3. Example of $I_c(\varepsilon)$ results and related data analysis obtained on densified Bi-2212 sample I-1 in the monotonic loading mode (I) at 16 T, 4.26 K, and 0.1 μV cm^{-1}. A linear fit is used to determine the onset of deviation from linearity, defined as ε_{irr}. Points selected to maximize the correlation factor R of the linear fit are plotted by use of square symbols for clarity. Value of the slope α of $I_c(\varepsilon)$ dependence within the reversible regime is indicated in the graph.

4.1.2. Mode III. An example of the results obtained in mode III is shown in figure 4 for sample III-1. The solid and empty circle symbols plotted on the left Y-axis represent $I_c(\varepsilon)$ when the sample is loaded and fully unloaded to zero applied-strain and are indicated by a pair of unprimed and primed letters, respectively. For example, A′ is the fully unloaded point that corresponds to the loaded point A. Unlike in mode II, the unloading strain step $\Delta\varepsilon$ is variable throughout the measurements (table 1). Note that the full unloading refers to zero strain of the spring device itself, not necessarily the sample strain. Upon straining the sample beyond its yield point and returning the spring to zero applied strain, the sample may be under some longitudinal compressive strain.

We used two data analysis methods for mode III as well. The first method utilizes the unloaded data points exclusively, and consists of calculating I_c relative degradation $(\Delta I_c/I_{c0})_R$ for each unloaded data point relative to the virgin value I_{c0} (at zero applied strain) and assigning to it the strain value of the

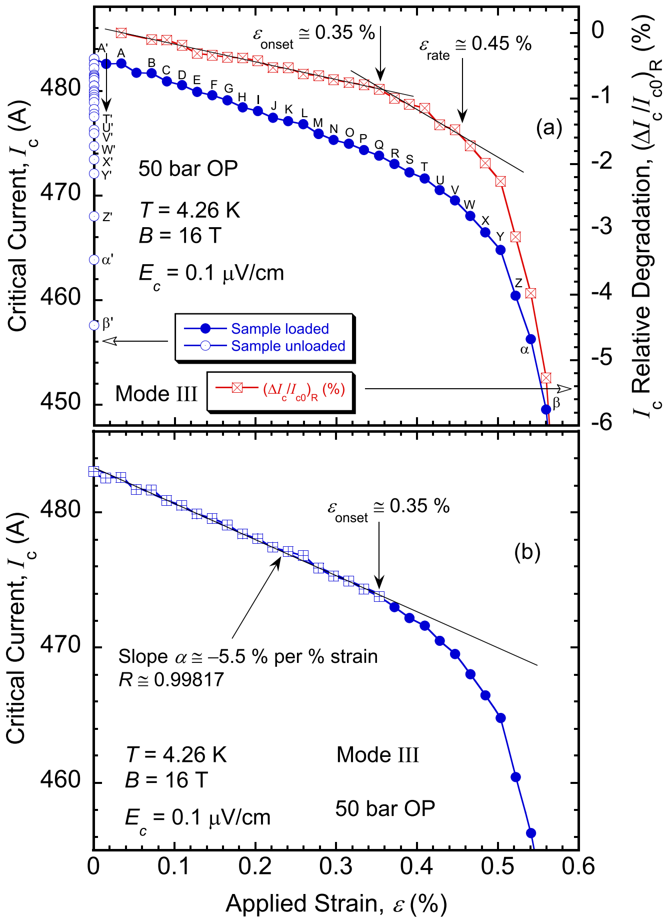

Figure 4. Example of $I_c(\varepsilon)$ results and related data analysis obtained on densified Bi-2212 sample III-1 in the load/full-unload mode (III) at 16 T, 4.26 K, and 0.1 μV cm^{-1}. (a) $I_c(\varepsilon)$ data for the sample when loaded and fully-unloaded to zero applied strain are plotted on the left Y-axis. Each pair of unprimed and primed letters indicates a loaded strain point (solid symbol) and its corresponding fully unloaded strain point (empty circle symbol), respectively (for example points A and A′). Degradation $(\Delta I_c/I_{c0})_R$ for the unloaded points relative to the virgin value I_{c0} is plotted on the right Y-axis as a function of ε by use of square symbols. It illustrates how I_c of the fully unloaded points deviates from I_{c0} as ε is applied and released. This method of data analysis revealed three distinct regions bordered by two characteristic strains ε_{onset} and ε_{rate} that correspond to the end of the linear and weak dependence on ε of $(\Delta I_c/I_{c0})_R$ and the first noticeable rate change of $(\Delta I_c/I_{c0})_R$ vs. ε, respectively. (b) Linear fit of the loaded points to determine the onset of $I_c(\varepsilon)$ deviation from linearity, defined at ε_{onset}. Points maximizing the correlation factor R of the linear fit are plotted by use of square symbols for clarity. Method of data analysis in (a) that uses unloaded points only and in (b) that uses loaded points only yield the same results for ε_{onset}. Value of the slope α of $I_c(\varepsilon)$ dependence within the moderate strain regime is indicated in the graph.

corresponding loaded data point. For example, $(\Delta I_c/I_{c0})_R$ for the unloaded strain point Z′ is assigned the strain value of the loaded data point Z. This quantity $(\Delta I_c/I_{c0})_R$ for the unloaded strain points is not the same as the total degradation $(\Delta I_c/I_{c0})_T$ that measures the total drop of I_c at a loaded strain point with respect to I_{c0}. For example, $(\Delta I_c/I_{c0})_R$ is the I_c drop for the point Z′ with respect to I_{c0}, whereas $(\Delta I_c/I_{c0})_T$ is the I_c drop for the point Z with respect to I_{c0}.

The dependence of $(\Delta I_c/I_{c0})_R$ on ε is plotted on the right Y-axis by use of rectangular symbols, and measures how I_c of the fully unloaded points deviates from I_{c0} as ε is applied and released. This dependence exhibited three distinct domains (figure 4(a)): First, $(\Delta I_c/I_{c0})_R$ was linear but very progressive as a function ε. Then $(\Delta I_c/I_{c0})_R$ started decreasing slightly more over a relatively narrow strain range before dropping noticeably when strain is increased further. Note that, apart from the first couple of points, I_c was in fact not reversible in this mode, unlike in mode II. Moreover, the slope α is steeper by 35% compared to that in modes I and II (table 1), indicating more decrease of I_c in the moderate strain range in mode III. Due to the practically absent $I_c(\varepsilon)$ reversibility in mode III, the first characteristic strain where $(\Delta I_c/I_{c0})_R$ loses linearity vs. ε is notated ε_{onset} (instead of ε_{irr}). The same three domains have been observed invariably for the three taps of sample III-1. Results are summarized in table 1.

This analysis revealed two characteristic strain values, ε_{onset} and ε_{rate} (marked by arrows in figure 4(a)), delimiting the intersections of the three domains. ε_{onset} is strain at the end of the linear and shallow dependence of $(\Delta I_c/I_{c0})_R$ on ε, and ε_{rate} is strain marking the first noticeable change of the degradation rate. We note that ε_{onset} is smaller on average than ε_{irr} in modes I and II. The average value of ε_{rate} is also smaller and the same is true for $\varepsilon_{5\%}$. The total decrease $(\Delta I_c/I_{c0})_T$ at ε_{onset} is about 2% (see table 1).

The second method we used to analyze data in figure 4 is applied to the loaded points only and examines the linearity of $I_c(\varepsilon)$ in the moderate strain range. A first selection of data points that can be fitted with a linear function was made and the correlation coefficient R of the least-square fit calculated. To refine the fit, some data points around the end of $I_c(\varepsilon)$ linear part were then either removed or added to the fit to maximize R. The results are shown in figure 4(b). Data points selected that provide the best linear fit (i.e. maximum R) are plotted by use of square symbols for clarity. Following the observations from the first analysis, the point where $I_c(\varepsilon)$ deviates from linearity is defined as ε_{onset} (not ε_{irr}). The value of ε_{onset} agreed very well with that determined from the first analysis applied to the unloaded data only (figure 4(a)). Here too, results from the two methods converged nicely.

As shown through data obtained in mode III, again, linearity of $I_c(\varepsilon)$ in the moderate strain range does not always necessarily mean reversibility of $I_c(\varepsilon)$. Linearity of $T_c(\varepsilon)$ in Bi-2212 material is expected to yield a linear dependence of $I_c(\varepsilon)$ [29, 30]. However, when the slope α exceeds a value around -4% per % strain (for densified samples), as for sample III-1 (see table 1), it is perhaps indicative of a convolution of elastic strain effects intrinsic to Bi-2212 material with irreversible strain effects that may arise from very mild and progressive damage such as microcracks in Bi-2212, as noted in [3].

4.1.3. Effect of the measurement mode. Comparison of the three measurement modes I, II, and III is presented in figure 5 where we display raw $I_c(\varepsilon)$ data (also see table 1). Modes I and II (with both $\Delta\varepsilon$ values of -0.11% and -0.15%) yielded very

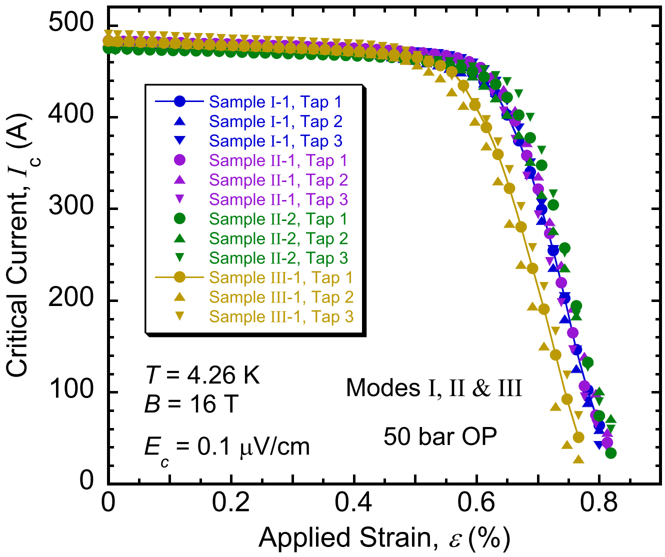

Figure 5. Comparison of raw $I_c(\varepsilon)$ data at 0.1 μV cm^{-1} for four densified Bi-2212 wire samples measured in the monotonic-loading, load/partial-unload, and load/full-unload modes (I, II, and III) at 16 T and 4.26 K. The results were very consistent, for all sample segments and over the whole range of strain applied, except for sample III-1 for which characteristic strains were smaller and $I_c(\varepsilon)$ entire curve was shifted to lower strain values. This may be indicative of some influence of mode III on the results obtained (also see appendix A). In contrast, modes I and II are equivalent, at least up to $\Delta\varepsilon = -0.15\%$.

consistent results, indicating that these two modes are equivalent, at least for $\Delta\varepsilon$ values within -0.15%. On the other hand, in mode III, $I_c(\varepsilon)$ curve was shifted to lower ε values in the steep degradation region, consistent with the smaller values of the characteristic strains obtained for sample III-1 (table 1). This indicates that mode III may have some influence on the data. Hence, specifying the mode of measurements used is pertinent for result evaluations and comparisons. We emphasize again that, in mode III, the sample may be forced into longitudinal compression upon unloading the spring to zero applied strain. This mode may not be representative of situations in magnets.

The absence of $I_c(\varepsilon)$ reversibility in mode III could be because, upon fully unloading the spring to zero applied strain, and even though the sample and spring were firmly soldered together, the sample may had been under some compressive strain if it had previously yielded in tension. In this case, irreversibility would not be due to tensile but to compressive strain. The other possibility is that this mode is simply more severe than mode II (and mode I) as the step $\Delta\varepsilon$ was variable and significantly bigger than -0.15% (that we chose for sample II-2) for most of the measurements in mode III. It is conceivable that mode II would not have shown reversibility either if the step $\Delta\varepsilon$ were chosen significantly bigger than -0.15%, even if kept constant. It is plausible (but not tested) that, starting from a certain value of $\Delta\varepsilon$ ($<-0.15\%$), data in mode II might converge with those in mode III.

It is worthwhile noting that the influence of mode III is only evident in the case of samples presenting a homogeneous response to strain, like these investigated herein (figure 5). As will be shown in appendix B for samples having non-uniform response to strain, the effect of measurement modes is not obvious. It is masked by sample inhomogeneity.

Among the three modes we tested, we prefer mode II because it allows checking $I_c(\varepsilon)$ reversibility in addition to the relative ease it offers for determining the conductor's characteristic strains. Mode III might be suitable for measuring conductors in more severe conditions, but it is likely not a substitute to fatigue-cycling tests.

4.1.4. Effect of the electric-field criterion E_c.

Many of the strain data reported in literature for Bi-2212 conductors used 1 μV cm^{-1} criterion. It is therefore useful to evaluate if E_c has an effect on the characteristic strains. In this section, we analyze $I_c(\varepsilon)$ data for I_c values obtained at 1 μV cm^{-1} in the same ways explained above. The results are summarized in table 2. By comparing tables 1 and 2, it appears that values of the characteristic strains obtained from I_c data at 1 μV cm^{-1} are slightly higher in general, by about 0.02%–0.04% strain, than those obtained from data at 0.1 μV cm^{-1}. Sometimes, these strains are the same within the analysis uncertainty. Also, the slope α is marginally shallower for data at 1 μV cm^{-1}. A typical example of this comparison is illustrated in figure 6, where plotted data are for sample II-2 in the loaded state (as in figure 1(b)). We conclude that the effect of E_c on extracted characteristic strains is small between 0.1 and 1 μV cm^{-1} .

4.2. Compressive strain effects in Mode I

Results obtained in longitudinal compressive strain are shown in figures 7(a) and (b) for sample I-c1. Figure 7(b) depicts the data subset delimited by the rectangle in figure 7(a). Measurements were obtained down to -1% strain, in mode I principally except that strain was fully unloaded once, at a small strain, to check reversibility (points A and A$'$ in figure 7(b)). The decrease of I_c with ε was progressive at moderate compressive strain. In fact, I_c was constant at first until the strain value $\varepsilon_{\mathrm{onset}} = -0.05\%$ where it started decreasing (figure 7(b)). Degradation of I_c is expected to be irreversible for most if not all of the compressive strain range. We did not check reversibility for strain points before point A, hence the labeling $\varepsilon_{\mathrm{onset}}$ instead of $\varepsilon_{\mathrm{irr}}$. Nonetheless, it is plausible that $I_c(\varepsilon)$ behaves reversibly along that narrow plateau, which would slightly expand the reversible tensile strain range. Degradation of I_c grew to about -40% at -1% strain. Nevertheless, total degradation remained significantly less than that obtained under tensile strain where it was close to -95% at around 0.8% strain (figure 5). The three taps of sample I-c1 exhibited very similar results (figure 7(a)), indicating that the sample remained firmly attached to the spring and did not delaminate from it during application of compressive strain.

The *n-value* dependence on ε is displayed in figure 8. Despite that I_c degraded to levels as high as 40% (figure 7(a)), *n-value* hardly changed with compressive strain. This result is in sharp contrast with the strong decrease of *n-value* with tensile strain (figure 2). This also reinforces our comment in

Table 2. Characteristic strains and related parameters obtained on densified Bi-2212 samples measured in modes I, II, and III at $E_c = 1\ \mu V\ cm^{-1}$.

Monotonic-loading mode (I)									
50 bar OP-HT		Slope α (% per % strain)	Coefficient R	ε_{irr} (%)	$(\Delta I_c/I_{c0})_T$ at ε_{irr} (%)	$\varepsilon_{2\%}$ (%)	ε_{rate} (%)	$(\Delta I_c/I_{c0})_T$ at ε_{rate} (%)	$\varepsilon_{5\%}$ (%)
Sample I-1	Tap 1	–3.8	0.99873	0.39	–1.5	0.46	—	—	0.59
$\Delta\varepsilon = 0\%$	Tap 2	–3.9	0.99906	0.39	–1.5	0.45	—	—	0.59
	Tap 3[a]	–3.6	0.99923	0.46	–1.7	0.50	—	—	0.61
Load/Partial-unload mode (II)									
50 bar OP-HT		Slope α (% per % strain)	Coefficient R	ε_{irr} (%)	$(\Delta I_c/I_{c0})_T$ at ε_{irr} (%)	$\varepsilon_{2\%}$ (%)	ε_{rate} (%)	$(\Delta I_c/I_{c0})_T$ at ε_{rate} (%)	$\varepsilon_{5\%}$ (%)
Sample II-1	Tap 1	–3.9	0.99915	0.40	–1.6	0.46	0.53	–2.6	0.61
$\Delta\varepsilon = -0.11\%$	Tap 2	–3.9	0.99931	0.43	–1.6	0.47	0.51	–2.4	0.61
	Tap 3	–4.0	0.99933	0.42	–1.6	0.46	0.49	–2.3	0.59
Sample II-2	Tap 1	–4.1	0.99812	0.44	–1.8	0.47	0.50	–2.4	0.60
$\Delta\varepsilon = -0.15\%$	Tap 2	–4.0	0.99823	0.44	–1.9	0.46	0.50	–2.4	0.59
	Tap 3	–3.9	0.99875	0.50	–2.0	0.50	0.56	–2.5	0.64
Load/Full-unload mode (III)									
50 bar OP-HT		Slope α (% per % strain)	Coefficient R	ε_{onset} (%)	$(\Delta I_c/I_{c0})_T$ at ε_{onset} (%)	$\varepsilon_{2\%}$ (%)	ε_{rate} (%)	$(\Delta I_c/I_{c0})_T$ at ε_{rate} (%)	$\varepsilon_{5\%}$ (%)
Sample III-1	Tap 1	–5.1	0.99875	0.35	–1.8	0.39	0.45	–2.5	0.55
$\Delta\varepsilon$ variable	Tap 2	–5.2	0.99831	0.33	–1.7	0.38	0.42	–2.4	0.52
	Tap 3	–5.1	0.99919	0.39	–2.0	0.39	0.45	–2.5	0.54

[a] See appendix A.

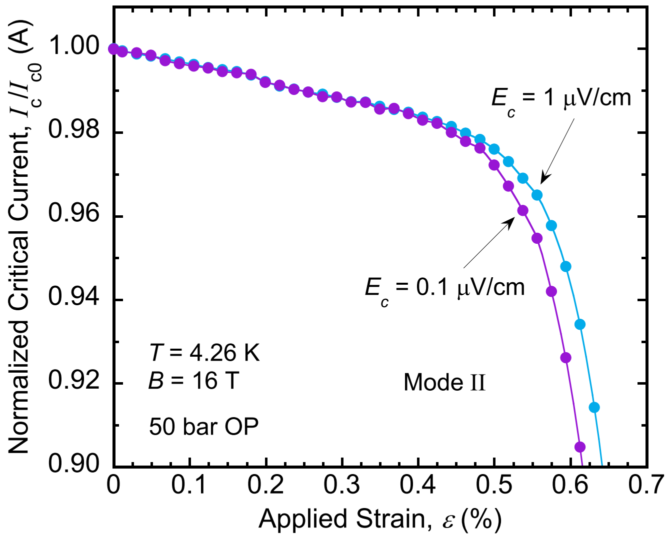

Figure 6. Comparison of normalized $I_c/I_{c0}(\varepsilon)$ data obtained at the two electric-field criteria 0.1 and 1 μV cm^{-1}, for sample II-2 measured in the load/partial-unload mode (II) at 16 T and 4.26 K. The curve $I_c/I_{c0}(\varepsilon)$ is shifted to higher strain values at 1 μV cm^{-1} and the corresponding characteristic strains are slightly higher by 0.02%–0.04% (sometimes not, as shown in tables 1 and 2). The slope α is marginally shallower for 1 μV cm^{-1}.

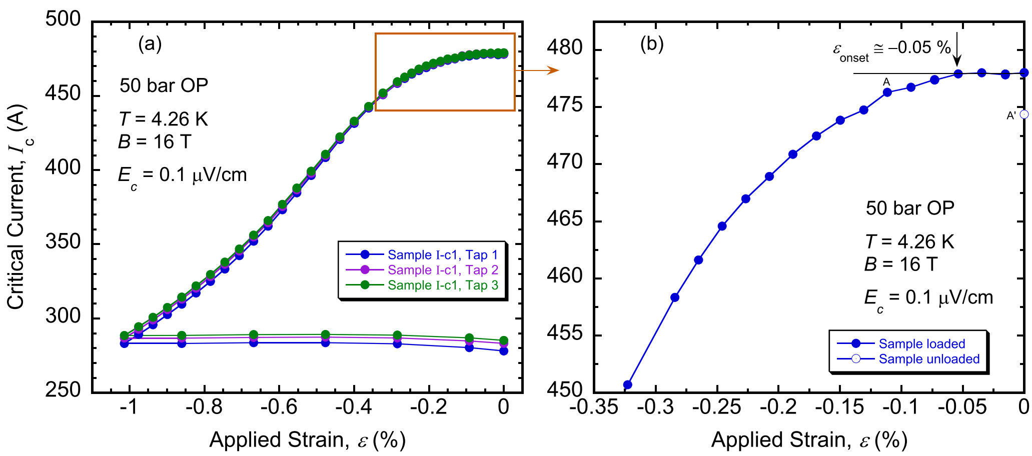

Figure 7. Results of $I_c(\varepsilon)$ at 0.1 μV cm^{-1} in longitudinal compressive strain down to -1% for densified Bi-2212 sample I-c1 measured mostly in the monotonic-loading mode (I) at 16 T and 4.26 K. (a) I_c degraded irreversibly with ε. Data highlighted by the rectangle are shown in detail in (b) indicating that $I_c(\varepsilon)$ was constant for small compressive strains down to $\varepsilon_{onset} \approx -0.05\%$ before it started degrading irreversibly.

section 4.1.1 on the difficulty of detecting the onset of irreversibility from *n-value* data. Buckling of Bi-2212 grains generated by longitudinal compression perhaps affects current paths along Bi-2212 filaments differently than crack defects produced in longitudinal tension.

5. Discussion and suggestions

The results and analysis presented in sections 4.1 and 4.2 are captured in figure 9, where representative datasets are combined for both tensile and compressive strain regimes. In this graph, we marked all the characteristic strains defined above along with the slope α. In the following, we discuss the main points of this paper and make a few recommendations:

(1) Besides figure 9, we tabulated the values of ε_{irr}, $\varepsilon_{2\%}$, ε_{rate}, and $\varepsilon_{5\%}$, as well as those of $(\Delta I_c/I_{c0})_T$ at ε_{irr} and ε_{rate} (see table 1), for all segments of all samples measured in the three modes to provide a detailed view of the results and to evaluate each strain-limit criterion used in literature for Bi-2212 conductors. Values for the 'strain limit' appear to span from about 0.4% if ε_{irr} is taken as the limit, to 0.6% if $\varepsilon_{5\%}$ is taken as the limit, for the same given Bi-2212 sample (measured in either modes I or II). Hence, different criteria/definitions yield a broad variation in the values extracted for the 'strain limit'. It is clear that these criteria/definitions should not be mixed or considered equivalent because they do not lead to the same result. Hence, it is quite pertinent that the definition used be made explicit when Bi-2212 strain data are reported.

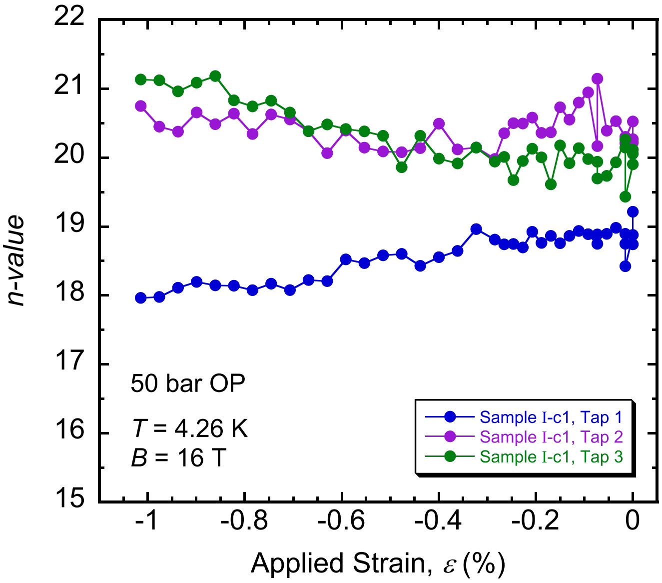

Figure 8. Results of n-$value(\varepsilon)$ in longitudinal compressive strain down to -1% for densified Bi-2212 sample I-c1, measured mostly in the monotonic-loading mode (I) at 16 T and 4.26 K. *n-value* remained essentially unchanged with ε despite the clear degradation of I_c shown in figure 7(a).

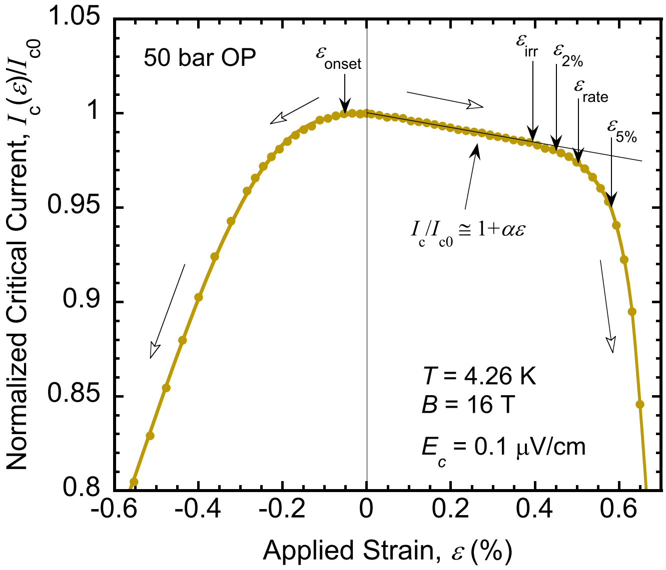

Figure 9. Representative Datasets of I_c/I_{c0} dependence on both longitudinal tension and compression, obtained on densified Bi-2212 samples at 16 T, 4.26 K, and 0.1 μV cm^{-1}. All characteristic strains $\varepsilon_{\rm irr}$, $\varepsilon_{2\%}$, $\varepsilon_{\rm rate}$, and $\varepsilon_{5\%}$ in tension, and $\varepsilon_{\rm onset}$ in compression, are marked by arrows. The graph shows a typical spread of the tensile 'strain limit' from 0.4% to 0.6% depending solely on its definition. This points to the need for a unified approach for Bi-2212 strain data acquisition and analysis for better consistency of the results reported in literature.

(2) We may not need to use a unique definition and report a unique characteristic strain, but we recommend the use of a unique labeling system. Unifying the labeling for each of the characteristic strains will remove ambiguities as to the meaning of the 'strain limit' reported and what it represents. For example, '$\varepsilon_{\rm irr}$' should only be used to mark the onset of $I_c(\varepsilon)$ irreversibility. If an I_c-degradation criterion is used instead, say $X\%$ degradation, then a label like '$\varepsilon_{X\%}$' would be more suitably representative of this parameter. It should not incorporate the term 'irr' so as to not signify that I_c remains reversible up to that I_c-degradation level. Such an assumption is not necessarily true and would be misleading otherwise. If a unique labeling system is adopted, then different definitions can be used that are within the resolution of a given strain apparatus, without the risk of misrepresentation. Afterall, it might be useful for magnet designers to know as many of the conductor characteristic strains as possible.

(3) It is evident that the 'strain limit' extracted through I_c-degradation criteria cannot be assimilated to $\varepsilon_{\rm irr}$. Reversibility of $I_c(\varepsilon)$ stops significantly before $\varepsilon_{5\%}$ is reached, for example. The progressive nature of I_c irreversible degradation beyond $\varepsilon_{\rm irr}$ might allow for designing magnets to operate at strains close to $\varepsilon_{5\%}$ but this needs to be demonstrated. Deciding what characteristic strain gives the proper measure of the conductor's strain resilience to safely design and operate magnets may need more investigations, such as fatigue cycling. Meanwhile, differentiating among these characteristic strains is needed, at least from metrology viewpoint.

(4) The percent I_c-degradation definition should be explicit whether it is relative or total and to what reference it is calculated.

(5) A unified approach for acquiring and analyzing $I_c(\varepsilon)$ raw data would allow objective data comparisons among different conductors and different labs. Feedback from such comparisons on the relations between the conductor's strain performance and the heat-treatment conditions, conductor design, or any other potentially relevant conductor parameter, or attempts to compare different strain apparatuses to find out which ones are most suitable, will likely not be all that reliable without a unified approach that would allow comparing together parameters of the same nature.

It is worthwhile mentioning the work of Osamura *et al* on Bi-2223 and ReBCO coated conductors where they compared the stress and strain limits defined at 99% recovery of I_c upon unloading the sample to zero strain and at 95% retention under strain of the virgin value I_{c0}, respectively [31]. From I_c measurements on straight samples at 77 K in self-field, they found that the I_c 95% retention is not a valid criterion for defining the irreversible stress and strain limits for Bi-2223 and ReBCO conductors. They proposed the 99% recovery of I_c as a practical criterion instead and used fatigue testing (up to 100 cycles) to validate this criterion. Our results do concur with their conclusion to not consider $\varepsilon_{5\%}$ as the irreversible strain limit. It would be very useful if common standard definitions can be developed for all these three conductors.

6. Conclusion

We described and compared protocols for measuring effects of longitudinal strain on transport properties in densified Bi-2112 round-wire samples. We examined methods for analyzing strain data to extract values of the irreversible strain limit $\varepsilon_{\rm irr}$ and other strains ($\varepsilon_{2\%}$, $\varepsilon_{\rm rate}$, and $\varepsilon_{5\%}$) characterizing $I_{\rm c}(\varepsilon)$ transition from weak to steeper strain dependences. $I_{\rm c}$-degradation criteria are often used to define the so-called 'strain limit', which is sometimes notated $\varepsilon_{\rm irr}$ by default.

We found that, even for physically the same sample, a strain limit can range from about 0.4% if it is $\varepsilon_{\rm irr}$ to about 0.6% if it is $\varepsilon_{5\%}$, thus changing significantly with the criterion used due to the gradual nature of $I_{\rm c}$ degradation in Bi-2212 conductors at $\varepsilon_{\rm irr} < \varepsilon < \varepsilon_{5\%}$. Therefore, at least from metrology standpoint, criteria in use are not equivalent and cannot possibly define the same parameter. Considering them similar leads to large errors. A distinction has to be made between $\varepsilon_{\rm irr}$ — the strain that marks the onset of $I_{\rm c}(\varepsilon)$ irreversibility — and any strain $\varepsilon_{X\%}$ where $I_{\rm c}$ degradation reaches a certain arbitrary level $X\%$. In fact, unified notations for these characteristic strains will be very helpful for eliminating definition ambiguities.

For the purpose of converging approaches in use, we proposed protocols and methodologies for acquiring and analyzing strain data for Bi-2212 conductors. These, or similar methodologies if consensually preferred, would make data comparisons straightforward and meaningful, and would offer a more solid platform for finding causalities between strain properties and conductor fabrication specificities. This does not necessarily mean that only one criterion should be used. In fact, results at multiple criteria can be reported as long as the respective characteristic strain is uniquely notated and the criterion used for it is explicitly defined, as in tables 1 and 2.

Data availability statement

The data that support the findings of this study are available upon reasonable request from the authors.

Acknowledgment

This work was supported by the U.S. Department of Energy, Office of Science, Office of High Energy Physics, Grant DE-SC0017657, the National High Magnetic Field Laboratory (NHMFL) supported by the National Science Foundation Cooperative Agreements DMR-1644779, DMR-2128556, and the State of Florida. We thank J Jiang, E Bosque, and L English, for preparing and heat-treating Bi-2212 samples. We also thank D Larbalestier for extensive discussions of the results.

Appendix A

In this appendix, we detail a rare behavior where $I_{\rm c}$ increased slightly as a function of tensile strain just before $\varepsilon_{\rm irr}$ and discuss how to analyze data when such behavior occurs. Among the 12 segments we measured in tension in all modes (see tables 1 and 2), this behavior happened in one segment only—tap 3 of sample I-1 (50 bar). This tap is marked by an asterisk in tables 1 and 2. We also have seen a similar behavior on a 5 bar specimen (sample I-3), which we include in this appendix to show that this behavior is likely not related to the densification of Bi-2212 filaments. Both samples were measured in the monotonic-loading mode I. This behavior is depicted in figures 10(a)–(c) for sample I-1 and in figures 10(d)–(f) for sample I-3, respectively.

As shown in figures 10(a) and (d), at 0.1 μV cm^{-1}, $I_{\rm c}(\varepsilon)$ deviated from linearity before $\varepsilon_{\rm irr}$ and increased slightly. This behavior did not occur at 1 μV cm^{-1}, as presented in figures 10(b) and (e). *n-value*(ε) also exhibited a slight increase before $\varepsilon_{\rm irr}$ for both samples (figures 10(c) and (f)), signaling a steepening of the corresponding I–V curves. It is this steepening that caused the slight increase of $I_{\rm c}(\varepsilon)$ at 0.1 μV cm^{-1}. We are unsure of its origin, nonetheless.

To analyze such data at 0.1 μV cm^{-1}, we selected the points that can be fitted with a linear function as to maximize the correlation factor R (as explained above). These points are plotted by use of square symbols in figures 10(a) and (d). A line parallel to this linear fit is drawn to meet the higher $I_{\rm c}$ points and $\varepsilon_{\rm irr}$ is defined where $I_{\rm c}(\varepsilon)$ starts deviating from this line. This method is validated by the analysis of $I_{\rm c}(\varepsilon)$ data at 1 μV cm^{-1}, which analysis yielded similar values for $\varepsilon_{\rm irr}$, as shown in figures 10(b) and (e). We note that values of $\varepsilon_{\rm irr}$ for these taps were among the highest (see tables 1 and 2).

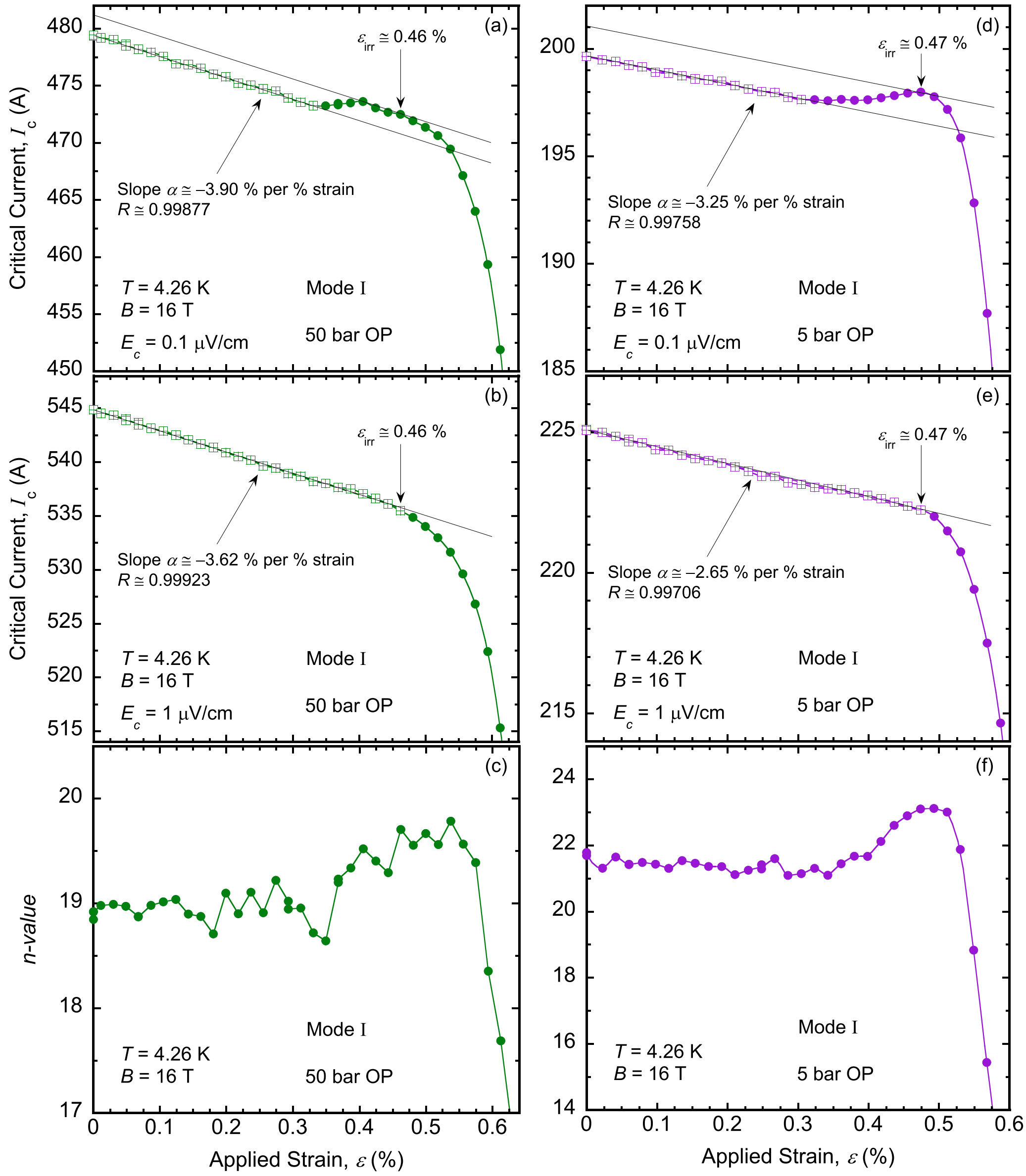

Figure 10. (a)–(b) depict $I_c(\varepsilon)$ at 0.1 and 1 μV cm^{-1}, respectively, and (c) *n-value*(ε) results obtained on tap 3 of densified (50 bar) sample I-1 in the monotonic-loading mode (I) at 16 T and 4.26 K. Similarly, (d)–(e) display $I_c(\varepsilon)$ at 0.1 and 1 μV cm^{-1}, respectively, and (f) *n-value*(ε) results obtained on a non-densified (5 bar) sample I-3 in the monotonic-loading mode (I) at 16 T and 4.26 K. (a)&(d) At 0.1 μV cm^{-1}, both taps show a slight increase of $I_c(\varepsilon)$ before ε_{irr}, caused by (c)&(f) a slight increase of *n-value*(ε) that indicates steepening of the corresponding *I–V* curves. Analysis of data when such behavior occurs is explained in appendix A.

Appendix B

In this appendix we give an example of inhomogeneous samples measured in modes I, II, and III. These samples were of the same wire PMM180410 but were subjected to a 5 bar OP-HT. From figure 11, it is evident that the non-uniform response of these samples to strain was significant enough that it masked any difference potentially related to the mode of measurements. We provide this example to nuance the results depicted in figure 5 for homogeneous samples where mode III appears to influence data obtained whereas modes I and II lead to very similar results.

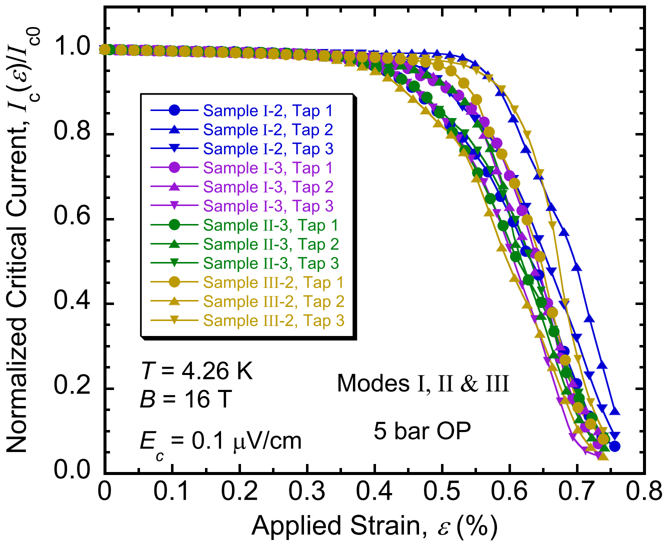

Figure 11. Comparison of normalized $I_c/I_{c0}(\varepsilon)$ data at 0.1 μV cm^{-1} for four 5 bar (non-densified) Bi-2212 wire samples measured in the monotonic-loading, load/partial-unload, and load/full-unload modes (I, II, and III) at 16 T and 4.26 K. The results were scattered, indicating an inhomogeneous response of these samples to strain along the sample length. Inhomogeneity was prominent enough to mask any effect of measurement modes on the data. This contrasts with the results in figure 5 for 50-bar (densified) samples where mode III yielded somewhat different results as compared to modes I and II.

ORCID iD

Najib Cheggour https://orcid.org/0000-0002-0741-3065

References

[1] Jiang J *et al* 2019 *IEEE Trans. Appl. Supercond.* **29** 6400405
[2] Larbalestier D C *et al* 2014 *Nat. Mater.* **13** 375–81
[3] Cheggour N, Lu X F, Holesinger T G, Stauffer T C, Jiang J and Goodrich L F 2012 *Supercond. Sci. Technol.* **25** 015001
[4] ten Haken B, Godeke A, Schuver H-J and ten Kate H H J 1996 *IEEE Trans. Magn.* **32** 2720–3
[5] ten Haken B, ten Kate H H J and Tenbrink J 1995 *IEEE Trans. Appl. Supercond.* **5** 1298–301
[6] ten Haken B and ten Kate H H J 1996 *Physica* C **270** 21–24
[7] Godeke A, Hartman M H C, Mentink M G T, Jiang J, Matras M, Hellstrom E E and Larbalestier D C 2015 *Supercond. Sci. Technol.* **28** 032001
[8] Bjoerstad R, Scheuerlein C, Rikel M O, Ballarino A, Bottura L, Jiang J, Matras M, Sugano M, Hudspeth J and Di Michiel M 2015 *Supercond. Sci. Technol.* **28** 062002
[9] Chen H, Liu H, Liu F, Shi Y, Jin H, Zhou C, Dai C, Li C, Qin J and Li J 2020 *IEEE Trans. Appl. Supercond.* **30** 6400304
[10] Dai C, Qin J, Liu B, Liu P, Wu Y, Nijhuis A, Zhou C, Li C, Hao Q and Liu S 2018 *IEEE Trans. Appl. Supercond.* **28** 6400104
[11] Sugano M, Itoh K and Kiyoshi T 2006 *IEEE Trans. Appl. Supercond.* **16** 1039–42
[12] Matras M R, Hellstrom E E, Trociewitz U P, Jiang J and Larbalestier D C 2019 *Densified superconductor materials and methods Patent* No. US010450641B2
[13] Matras M R, Jiang J, Trociewitz U P, Larbalestier D C and Hellstrom E E 2020 *Supercond. Sci. Technol.* **33** 025010
[14] Huang Y, Miao H, Hong S and Parrell J A 2014 *IEEE Trans. Appl. Supercond.* **24** 6400205
[15] Kametani F *et al* 2011 *Supercond. Sci. Technol.* **24** 075009
[16] Jiang J, Starch W L, Hannion M, Kametani F, Trociewitz U P, Hellstrom E E and Larbalestier D C 2011 *Supercond. Sci. Technol.* **24** 082001
[17] Scheuerlein C, Di Michiel M, Scheel M, Jiang J, Kametani F, Malagoli A, Hellstrom E E and Larbalestier D C 2011 *Supercond. Sci. Technol.* **24** 115004
[18] Walters C R, Davidson I M and Tuck G E 1986 *Cryogenics* **26** 406–12
[19] Cheggour N and Hampshire D P 2000 *Rev. Sci. Instrum.* **71** 4521–30
[20] Goodrich L F, Cheggour N, Stauffer T C, Filla B J and Lu X F 2013 *J. Res. Natl Inst. Stand. Technol.* **118** 301–52
[21] Cheggour N, Stauffer T C, Starch W, Lee P J, Splett J D, Goodrich L F and Ghosh A K 2018 *Sci. Rep.* **8** 13048
[22] Cheggour N, Stauffer T C, Starch W, Goodrich L F and Splett J D 2019 *Sci. Rep.* **9** 5466
[23] Distin J S, Motowidlo L R, Lee P J, Larbalestier D C, Ghosh A K, Lu X F, Cheggour N, Stauffer T C and Goodrich L F 2011 *IEEE Trans. Appl. Supercond.* **21** 2529–32
[24] Cheggour N, Ekin J W and Thieme C L H 2005 *IEEE Trans. Appl. Supercond.* **15** 3577–80
[25] Ekin J W 1980 *Cryogenics* **20** 611–24
[26] Godeke A, Dhalle M, Morelli A, Stobbelaar L, van Weeren H, van Eck H J N, Abbas W, Nijhuis A, den Ouden A and ten Haken B 2004 *Rev. Sci. Instrum.* **75** 5112–8
[27] Cheggour N and Marks E L 2020 On the need for protocols and standard procedures for studying $I_c(\varepsilon)$ in Bi-2212 wires (available at: www.researchgate.net/publication/348480515_On_the_Need_for_Protocols_and_Standard_Procedures_for_Studying_Icstrain_in_Bi-2212_Wires)
[28] Goodrich L F, Cheggour N, Lu X F, Splett J D, Stauffer T C and Filla B 2011 *Supercond. Sci. Technol.* **24** 075022
[29] Chen X-F, Tessema G X and Skove M J 1991 *Physica* C **181** 340–4
[30] Lu X F, Goodrich L F, van der Laan D C, Splett J D, Cheggour N, Holesinger T G and Baca F J 2012 *IEEE Trans. Appl. Supercond.* **22** 8400307
[31] Osamura K, Machiya S and Nishijima G 2016 *Supercond. Sci. Technol.* **29** 094003